ACS OMEGA

http://pubs.acs.org/journal/acsodf

Article

Theoretical Study of Actinide Complexes with Macropa

Attila Kovács*

Cite This: *ACS Omega* 2020, 5, 26431−26440

Read Online

ACCESS | Metrics & More | Article Recommendations | Supporting Information

ABSTRACT: The complex formation of actinium (Ac^{3+}) and californium (Cf^{3+}) ions with macropa (a promising ligand for medical applications, e.g., in targeted α therapy) has been studied by means of density functional theory (DFT) calculations. This work is focused on the structural and bonding properties, the latter on the basis of charge transfer data and topological properties of the electron density distribution. The effect of water solvent on the energetics has been investigated using the SMD model. A comparative analysis with the related properties of two representative lanthanide (La, Lu) complexes has been performed.

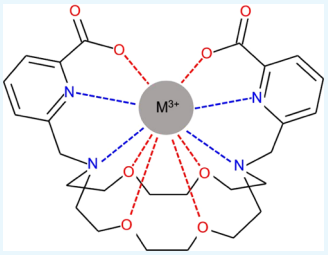

INTRODUCTION

The actinides (An) are best known for their applications in nuclear weapons and for energy production. However, their radioactivity can make them a very useful tool in nuclear medicine too. Their α-emitting isotopes ^{225}Ac[1−4] and ^{227}Th[5−8] are at an advanced level of clinical tests for the treatment of a range of cancers by means of targeted α therapy (TAT). Convincing results have been obtained for the treatment of metastatic castration-resistant prostate cancer,[9−11] acute myeloid leukemia,[12,13] neuroendocrine tumors,[14] and tumors expressing mesothelin.[15] The α-emitting radioisotope of uranium (^{230}U) is also a promising candidate for TAT based on its short half-life of 20.83 days.[16] For this actinide, however, an important issue is to find suitable chelating agents for stable binding of UO_2^{2+} under in vivo conditions.[17,18] In addition, ^{252}Cf is also considered for the treatment of cancer. The slow spontaneous fission of this radioisotope provides neutron radiation suitable for brachytherapy or internal radiation therapy.[19,20]

The radioisotopes are generally administered in a chelated form. The chelators for these ions are conjugated to a biological targeting vector (antibody or peptide), which transports them to the desired location in vivo. For such applications, the chelator ligands must possess two important properties:[21] (i) they should rapidly complex the metal ion under mild pH and temperature conditions and (ii) they should form highly stable complexes. The latter requirement is of paramount importance to prevent the redistribution of these toxic metal ions throughout the patient.

The design of suitable chelating agents for f-block elements is hampered by the electrostatic nature of their bonding interactions. Their low charge density results mostly in long and weak metal-donor bonds with the consequence of the low stability of these complexes. Hitherto, only a few promising chelators are available for lanthanides (Ln) and actinides. The most widely used chelator for lanthanides is the tetraazamacrocycle 1,4,7,10-tetraazacyclododecane-1,4,7,10-tetraacetic acid (DOTA) forming stable complexes with the small-size Ln ions.[22,23] A disadvantage of DOTA for larger ions (e.g., light An) is that the stability decreases with the size significantly. Nevertheless, for the time being, DOTA is the ligand of choice for linking of ^{225}Ac to biomolecules and has been successfully applied in several clinical tests.[24] In the meantime, search for improved chelators for An is ongoing.

Macrocycles based on the 1,7,10,16-tetraoxa-4,13-diazacyclooctadecane (D18C6) core show a thermodynamic preference for large over small metal ions.[25−32] Recently, a D18C6-based macrocycle possessing two picolinate arms (*N*,*N*′-bis[(6-carboxy-2-pyridil)methyl]-4,13-diaza-18-crown-6, macropa, Figure 1) has been shown to form rapidly a stable complex with ^{225}Ac^{3+}, the largest 3+ ion in the Periodic Table.[33] Macropa was also found to selectively bind large lanthanide,[34] alkaline

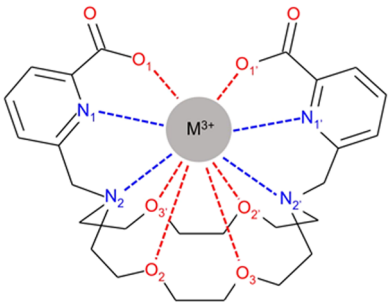

Figure 1. $M(L)^+$ complex with the numbering of selected atoms. In C_2 symmetry, the X_n and $X_{n'}$ atoms are equivalent.

Received: June 16, 2020
Accepted: July 20, 2020
Published: October 6, 2020

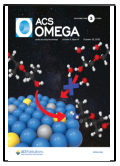

https://dx.doi.org/10.1021/acsomega.0c02873
ACS Omega 2020, 5, 26431−26440

earth,[35,36] and p-block[35] metal ions over their smaller analogues. The selectivity for the large An and Ln ions was found to be superior to related diaza[18]crown-6[25,28] and diaza[15]crown-5 derivatives.[37,38] This rare reverse size selectivity of macropa makes it a distinguished candidate for medical applications, where efficient chelators for large metal ions are highly needed. The clinical tests of Ac(macropa) derivatives are in progress with promising results: recently, a single dose of ^{225}Ac-RPS-074, an ^{225}Ac(macropa) bifunctional construct designed against prostate cancer, induced complete tumor ablation in mice.[39]

The present theoretical study aims to uncover the bonding of macropa (H_2L) with f elements. The reverse stability trend along the Ln series in aqueous solution (La > Lu) has been detected by potentiometric measurements[34] and interpreted on the basis of density functional theory (DFT) calculations.[40] The usually observed trend in the stability of gas-phase Ln complexes is the increase from La to Lu due to the increasing charge density of the metal ion in this order. (The latter being the result of the decreasing size of Ln^{3+} ions due to the Ln contraction.) In aqueous solutions, however, the hydration energy can introduce significant effects. It was shown in ref 40 that the balance between the increasing binding energies in the $Ln(L)^+$ complexes and the variation of the hydration energies across the lanthanide row was dominated by the increasing hydration energies of the Ln^{3+} ions, being therefore responsible for the reversed trend in the stability constants of these complexes in aqueous solution.

The importance of actinides in TAT calls for detailed information on the physicochemical properties of their complexes with the macropa ligand. There can be differences compared to lanthanides not only because of the size but also in the bonding due to the chemically more active 5f subshell. In the present study, macropa complexes with Ac^{3+}, Cf^{3+}, La^{3+}, and Lu^{3+} will be compared on the basis of DFT calculations. The properties in focus are the relative stabilities of these ionic $M(L)^+$ complexes, the effect of water solvation, and the characters of the main bonding interactions. The extra H_2O solvent molecule coordinating to La in the crystal structure of La(macropa),[33] similar to dimethylformamide (DMF) with Ba(macropa)[36] and in related complexes,[29,32,41,42] is not considered in the present comparative study. These small solvent molecules are supposed to fill the 11th coordination site of large M ions and accordingly, they were not observed with small metal ions, such as Lu^{3+}.[33] It should be noted, however, that the water molecule of $La(HL)(H_2O)^{2+}$ has not yet been confirmed in aqueous solution. These 11-coordinate complexes have a different structure in which one of the ligand picolinate arms is protonated, changing in this way the bonding properties of this COO group. While the overall thermodynamic stability of the complexes should be increased by the additional coordination, the macropa−M interaction is likely weakened with respect to 10-coordinate M(macropa) because of the changed COO−M bonding and the steric effects of the additional ligand molecule.

COMPUTATIONAL DETAILS

The computations were performed with the Gaussian09 suit of programs[43] using the hybrid metageneralized TPSSh exchange−correlation functional[44] in conjunction with quasi-relativistic pseudopotentials of the Stuttgart−Cologne group. The selection of the TPSSh functional was based on its good performance for the geometries and stability properties of Ln complexes[40,45,46] and accurate ^{17}O A^{iso} values of coordinated water molecules in various Gd complexes.[47] For H, N, C, and O, the standard 6-31G(dp) basis set was used. For the lanthanides and actinides, both the large-core and small-core quasi-relativistic pseudopotentials, LCPPs and SCPPs, respectively, were probed. The 4f-in-core LCPPs[48,49] for La and Lu (ECP46MWB and ECP60MWB, respectively) were coupled with a [7s6p5d]/[5s4p3d] valence basis set treating the 5s5p5d6s electrons.[48] The 4f-in-valence SCPPs (ECP28MWB)[50] had a segmented valance basis set with a contraction scheme of [14s13p10d8f6g]/[10s8p5d4f3g] treating the 4th, 5th, and 6th shells.[51] For Ac and Cf, the primary basis was the 5f-in-valence SCPPs (ECP60MWB)[52] in conjunction with valence basis sets having a contraction scheme of [14s13p10d8f6g]/[10s9p5d4f3g].[53,54] This choice was rationalized by the larger importance of the 5f electrons in the interactions of actinides compared to the intact 4f subshell in lanthanides. However, calculations with SCPPs can be considerably difficult due to SCF convergence problems. In the present study, SCF convergence failed for four conformers of $Cf(L)^+$ and in basis set superposition error (BSSE) calculations for the Cf and Ac complexes. No such problems occurred with the 5f-in-core LCPPs[55] (ECP78MWB and ECP87MWB for Ac and Cf, respectively) used in conjunction with a [7s6p5d2f1g]/[6s5p4d2f1g] valence basis set.[55] The application of the f and g polarization functions with the latter LCPPs (in contrast to their neglect in the recent literature on $Ln(L)^+$ complexes[34,40,45,56]) is in accordance with the mentioned larger importance of the 5f electrons in the interactions of actinides. The LCPP calculations provided data very close to the SCPP ones for $Ac(L)^+$, however, with small deviations for $Cf(L)^+$.

The ground state of the computed complexes was verified utilizing the STABLE keyword of the Gaussian09 code. Due to their closed-shell nature, spin-restricted calculations were performed for the Ac, La, and Lu complexes as well as for $Cf(L)^+$ with LCPP. With SCPP, the sextet ground state of open-shell $Cf(L)^+$ was treated using the spin-unrestricted formalism. BSSE was evaluated using the counterpoise method.[57] The solvent effects were taken into account using the polarizable continuum model (PCM)[58,59] with radii and nonelectrostatic terms for Truhlar and co-workers' SMD solvation model.[60] For the La^{3+} and Lu^{3+} ions, the PCM radii (1.874 and 1.659 Å, respectively) from ref 40 were used. The respective PCM radii for Ac^{3+} and Cf^{3+} were optimized in the present study to achieve an agreement with the hydration free energies in the literature.[61] No scaling factor (α = 1.0) was used for the PCM radii.

The atomic charges and charge transfer (CT) properties were calculated according to natural bond orbital (NBO) theory[62] utilizing the NBO 6.0 code.[63] The topological analysis of the electron density distribution according to the "quantum theory of atoms in molecules" (QTAIM)[64] was performed by means of the AIMAll software.[65] These bonding models are widely used for the assessment of bonding trends in organometallic complexes of f elements.[66−78]

RESULTS AND DISCUSSION

The stability of metal complexes in solution is determined by the following two main factors: (i) the binding energy of the ligand to the metal ions and (ii) the hydration energies of the complexes and free metal ions. In the following sections, these two factors are analyzed in detail: in the Structure and Bonding section, the conformational properties, energetics, and bonding in the gas-phase structures, while in the Energetics in Aqueous

https://dx.doi.org/10.1021/acsomega.0c02873
ACS Omega 2020, 5, 26431−26440

Solution section, the energies of hydration using the gas-phase reference structures.

Structure and Bonding. The complex formed by macropa with metals is presented in Figure 1. In the shown syn conformation of the ligand side arms, the metal ion is able to bind to all of the 10 donor atoms. The chiral complex can form 16 possible conformations (eight enantiomeric pairs of diastereoisomers) with C_2 symmetry. In a nonchiral environment, enantiomers possess the same physiochemical properties, hence the study of the eight diastereoisomeric forms is sufficient. The conventional nomenclature is X(yyy)(yyy), where X = Δ or Λ (absolute configurations of the picoline pendant arms) and y = δ or λ (absolute configurations of the six five-membered chelate rings formed in the complex).[79,80] To keep consistency with the literature, the present article deals with the eight Δ(yyy)(yyy) conformers. As the $La(L)^+$ and $Lu(L)^+$ complexes are well described in the literature,[34,40] only two of their relevant $\Delta(\delta\lambda\delta)(\delta\lambda\delta)$ and $\Delta(\lambda\delta\lambda)(\lambda\delta\lambda)$ conformers are included in the present comparative analysis.

The relative Gibbs free energies are presented in Figure 2, from which the solvation data are discussed in the Energetics in

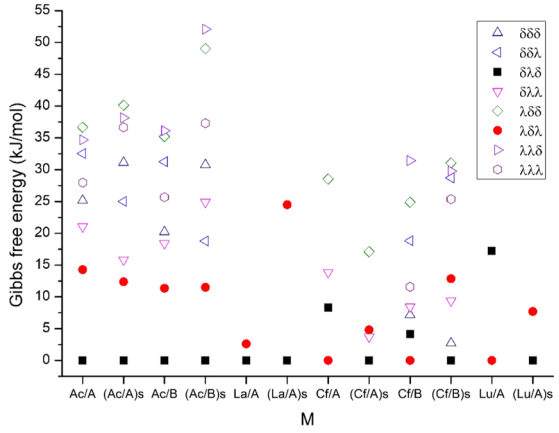

Figure 2. Relative Gibbs free energies of the eight $M(L)^+$ conformers in the gaseous phase and aqueous solution. At the *x* axis, the notations A, B, and s refer to SCPP and LCPP basis sets and aqueous solution, respectively. The conformers Δ(yyy)(yyy) are abbreviated by the yyy terms.

Aqueous Solution section. The effect of BSSE (where available) on the relative energies was a few kJ/mol; these data are given in Table S1 of the Supporting Information.

The ionic radii of the four f elements decrease in the order $Ac^{3+} > La^{3+} > Cf^{3+} > Lu^{3+}$ (the experimental 6-coordinate ionic radii being 1.12, 1.032, 0.95, and 0.861 Å, respectively).[81] In agreement with expectations based on related literature,[30,34] the present calculations predicted the preference of the $\Delta(\delta\lambda\delta)(\delta\lambda\delta)$ conformer for the large Ac^{3+} ion (similar to that for La^{3+}) and the preference of the $\Delta(\lambda\delta\lambda)(\lambda\delta\lambda)$ one for the smaller Cf^{3+} ion (similar to that for Lu^{3+})[30,34] in the gaseous phase. Calculations with SCPPs and LCPPs agreed with these relative stabilities. Regarding the other conformers, the energy differences predicted by the two pseudopotentials are quite similar for $Ac(L)^+$, while the agreement (by SCPP) is somewhat worse for the four obtained conformers of $Cf(L)^+$, referring to the role of the 5f electrons in the latter complex.

The energetic preference of the $\Delta(\delta\lambda\delta)(\delta\lambda\delta)$ conformer is well pronounced for $Ac(L)^+$ (with the largest M^{3+} radius) and similarly the preference of the $\Delta(\lambda\delta\lambda)(\lambda\delta\lambda)$ conformers for $Lu(L)^+$ (with the smallest ionic radius). For $La(L)^+$ and $Cf(L)^+$ (with ionic radii in between), the gas-phase energy differences between the two conformers are smaller.

The metal−ligand interactions are analyzed in the two most significant conformers $\Delta(\delta\lambda\delta)(\delta\lambda\delta)$ and $\Delta(\lambda\delta\lambda)(\lambda\delta\lambda)$ on the basis of molecular geometries and properties from the NBO[62] and QTAIM[64] bonding models. The analysis is based on the gas-phase reference geometries obtained with SCPP (taking into account the effect of f valance orbitals in Ac, La, and Cf). Geometry optimizations with LCPP including BSSE indicated marginal effects of BSSE for the main interatomic distances (in general a few thousandths of Å).

The metal−ligand bond distances are presented in Figure 3. Most of them agree within a few hundredths to 0.1 Å with the X-

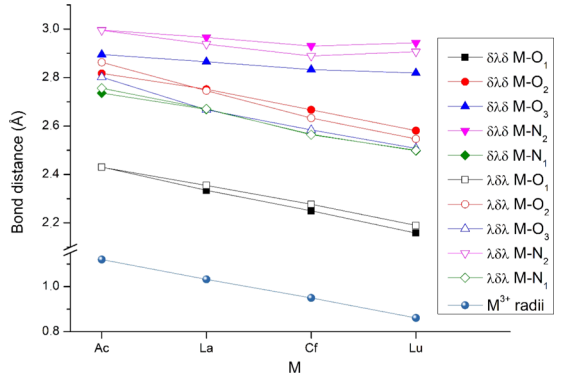

Figure 3. Selected bond distances of the $\Delta(\delta\lambda\delta)(\delta\lambda\delta)$ and $\Delta(\lambda\delta\lambda)$-$(\lambda\delta\lambda)$ conformers computed at the TPSSh/SCPP level.

ray crystal structure data[33] of $La(HL)(H_2O)^{2+}$ and $Lu(L)^+$ (cf. Table S2), whose experimental structures are less symmetric and the La complex contains an additional H_2O ligand. The changes induced by H_2O in the latter structure may mainly be responsible for the experimental La−O_1 distances being longer by ca. 0.2 Å than the computed ones.

For most of the presented computed bond distances, good correlation can be observed with the depicted M^{3+} ionic radii. Exceptions are the M−N_2 bonds of both conformers and the M−O_3 bond of the $\Delta(\delta\lambda\delta)(\delta\lambda\delta)$ conformer, which shorten only marginally. These are the longest coordinative bonds, i.e., the weakest ones; it is therefore reasonable that they accommodate to a less extent the change of the metal ion size. Most presented coordinative bonds have very close values in the two conformers, except for the M−O_3 one. This bond is considerably shorter in the $\Delta(\lambda\delta\lambda)(\lambda\delta\lambda)$ conformer, its length being comparable to the other M−O coordinative bonds.

From the 10 coordinative bonds, the strongest bonding with M^{3+} is created by the anionic carboxylate oxygens (O_1). These bonds are by 0.3−0.7 Å shorter than the bonds with the neutral (though polarized) O and N atoms. The second shortest coordinative bond is the one with the pyridine N_1. Hence, the leading role in the complex formation may be played by these M−O_1 and M−N_1 interactions.

The analogous Ac−O and Ac−N distances in the two $Ac(L)^+$ conformers are very close, suggesting bonding interactions of similar strength in contrast to the other three f elements, where larger differences can be observed. Based on its size, the Ac^{3+} ion may fit (nearly) equally into the cavity of the two L^{2-} conformers. The energetic preference of the $\Delta(\delta\lambda\delta)(\delta\lambda\delta)$

https://dx.doi.org/10.1021/acsomega.0c02873
ACS Omega 2020, 5, 26431−26440

Table 1. Dissociation Gibbs Free Energies and Selected QTAIM and NBO Data for the $\Delta(\delta\lambda\delta)(\delta\lambda\delta)$ and $\Delta(\lambda\delta\lambda)(\lambda\delta\lambda)$ Conformers of the $M(L)^+$ Complexes

[a]	$Ac(L)^+$		$La(L)^+$		$Cf(L)^+$		$Lu(L)^+$	
property[a]	$\delta\lambda\delta$	$\lambda\delta\lambda$	$\delta\lambda\delta$	$\lambda\delta\lambda$	$\delta\lambda\delta$	$\lambda\delta\lambda$	$\delta\lambda\delta$	$\lambda\delta\lambda$
q_M	+2.00	+2.00	+1.74	+1.68	+1.79	+1.72	+1.91	+1.85
q_{O_1}	−0.91	−0.91	−0.82	−0.81	−0.84	−0.83	−0.88	−0.87
∑LUAO	1.00	1.00	1.26	1.32	1.21	1.28	1.09	1.15
pop(6s/7s)	0.14	0.14	0.16	0.17	0.20	0.21	0.19	0.20
pop(5d/6d)	0.49	0.50	0.91	0.95	0.81	0.88	0.88	0.94
pop(4f/5f)[b]	0.23	0.22	0.18	0.19	0.11	0.10	0.0	0.0
E_{CT} (L → M)	1667	1671	3551	3969	3020	3447	2709	3068
E_{CT} (M → L)					26	30		
ΔM	1.15	1.15	1.18	1.22	1.27	1.33	0.98	1.03
∑DI	1.04	1.04	1.07	1.10	1.14	1.20	0.89	0.93
ΔG_{diss}	3966	3951	4104	4001	4323	4332	4451	4468

[a]Selected natural atomic charges, q (e); sum of populations of the lowest unoccupied atomic orbitals of M^{3+}, ∑LUAO (e); valence orbital populations of M, pop (e); second-order perturbation energies, E_{CT} (kJ/mol); difference between the integrated electron density and localization index of the atomic basin of M, $\Delta(M)$ (e); sum of the delocalization indices between M and L, ∑DI (e); and Gibbs free energies of dissociation without BSSE correction, ΔG_{diss} (kJ/mol). The conformers $\Delta(yyy)(yyy)$ are abbreviated by the yyy terms. [b]Number of excess electrons with respect to the M^{3+} ground state.

conformer may mainly be due to the smaller strain in this ligand geometry (cf. Figure S1 in the Supporting Information).

Further inspection of Figure 3 aimed to find correlations with the relative stabilities of the $\Delta(\delta\lambda\delta)(\delta\lambda\delta)$ and $\Delta(\lambda\delta\lambda)(\lambda\delta\lambda)$ conformers of the other complexes. The relative stability does not seem to be determined by the (strongest) $M-O_1$ interaction, whose bond length is slightly shorter in all of these $\Delta(\delta\lambda\delta)(\delta\lambda\delta)$ conformers. A similar conclusion can be drawn for the strain energies of the L^{2-} ligand, which are consistently larger by 20−30 kJ/mol in the $\Delta(\lambda\delta\lambda)(\lambda\delta\lambda)$ conformer (cf. Figure S1). The most prominent correlation with the increasing relative stability of the $\Delta(\lambda\delta\lambda)(\lambda\delta\lambda)$ conformer is the significant strengthening of the $M-O_3$ interaction in the latter conformer, as indicated by this bond distance (cf. Figure 3). The $M-O_2$ and $M-N_2$ bond distances also become shorter from Ac to Lu, but the changes are rather small.

Table 1 compiles selected results from the NBO[62,63] and QTAIM[64] analyses. The natural atomic charges (from NBO) of the metals are between +1.7 and +2.0, in agreement with a major ionic character of the metal−ligand bonding. At the same time, they indicate a considerable CT (1.0−1.3e) to M^{3+}, too. The transferred amount of electrons is represented by the population of lowest unoccupied atomic orbitals (LUAOs) of M^{3+}. These valence s, d, and f orbitals, being empty in the ion, serve as the acceptor orbitals in the $L^{2-} \rightarrow M^{3+}$ charge transfer. Altogether, the largest electron transfers occur in $La(L)^+$ and $Cf(L)^+$, while the strongest ionic bonding appears in $Ac(L)^+$. As the atomic charges of the donor O and N atoms indicate, the ionic interaction is particularly strong with O_1, its charge being close to the formal charge of the carboxylate anion.

The populations from the natural atomic orbital (NAO) scheme give information on the distribution of the transferred charge between the M valence (s, d, f) orbitals. In agreement with the expectations, the main CT acceptor orbitals are the valence d orbitals of M, with populations around 0.5e in Ac and around 0.9e in the other metals. Populations of the valence s and excess electrons on the f orbitals are between 20 and 30% of those of the valence d orbitals. While the Ac 5f orbitals are somewhat more involved in CT than the 7s, in Cf the trend is turned over due to the energetic stabilization of the 5f orbitals in the latter An.

The energy gain from CT can be assessed on the basis of the second-order perturbation energies from the NBO analysis. In agreement with the M valence orbital populations, the weakest CT occurs in $Ac(L)^+$, the CT energy being ca. half of those in the other three complexes. Among the latter three, the strongest interaction occurs in $La(L)^+$ while the weakest in $Lu(L)^+$. M → L back-donation was observed only in $Cf(L)^+$, even this one being marginal. Decomposition of the CT energies to donor−acceptor atom pairs is given in Figure 4. Most pronounced is the

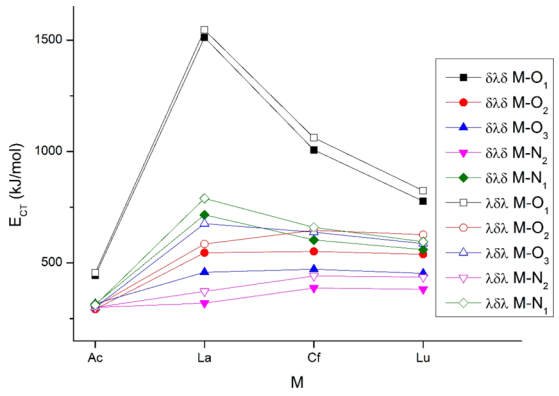

Figure 4. Main second-order perturbation energies from NBO analysis of the $\Delta(\delta\lambda\delta)(\delta\lambda\delta)$ and $\Delta(\lambda\delta\lambda)(\lambda\delta\lambda)$ conformers.

CT from O_1, while the CT energies from the other donors are close and partly overlap. The relative strengths of CTs in terms of the different metals agree qualitatively with the amount of transferred electrons (cf. Table 1).

The above shown main CT features are also reflected in the integral QTAIM parameters. In this model, the total transferred electrons from L^{2-} to M^{3+} are described by the amount of unlocalized electrons on M (denoted as ΔM in Table 1, obtained as the difference of the integrated electron density and localization index of the atomic basin of M). The basically different QTAIM and NBO models agree in the amount of the transferred electrons of ca. 1e in the complexes and in the trends within the Ln and An rows being Ac < Cf and La > Lu. However, deviation between QTAIM and NBO can be observed when

https://dx.doi.org/10.1021/acsomega.0c02873
ACS Omega 2020, 5, 26431−26440

comparing the two f element rows: the NBO model predicts a larger difference between the LUAO populations of Ln and An than that obtained in the ΔM values. Thus, from the four metals, QTAIM predicted the largest amount of transferred electrons in $Cf(L)^+$, while NBO in $La(L)^+$. This disagreement between the two models can also be seen in Figures 4 and 5.

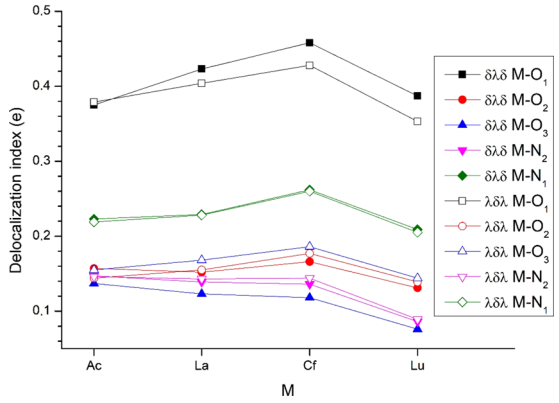

Figure 5. Delocalization indices from QTAIM analysis between selected atom pairs of the $\Delta(\delta\lambda\delta)(\delta\lambda\delta)$ and $\Delta(\lambda\delta\lambda)(\lambda\delta\lambda)$ conformers.

Another important property from the QTAIM analysis is the delocalization index (DI). This integral parameter quantifies the average number of electrons shared between two atoms connected by a bond path, i.e., forming the covalent bond.[72] The sum of the delocalization indices around each M is given in Table 1, while the DI data between the M−O/N atom pairs are presented in Figure 5. In agreement with the second-order perturbation energies from NBO analysis (Figure 4), the M^{3+} ions form the most extensive electron-sharing interactions with O_1 (ca. 0.4e). Considerably weaker (but still pronounced) are the interactions with N_1 (ca. 0.23e), while the interactions with the other donors have somewhat smaller DIs.

Bond critical points (BCPs) were located for all of the above 10 coordinative bonds (Figure 6). In addition, a few weak O···H and N···H hydrogen bonds were found in both conformers, contributing to the overall stability of the complexes.

Both the small electron density (ρ) and the positive Laplacian of the electron density ($\nabla^2\rho$) values (given in Figures S2 and S3 in the Supporting Information) refer to predominant ionic interactions between M and the heteroatoms in all complexes. Variations of these topological parameters of the BCPs are more or less consistent with those of the delocalization indices. The two significant differences include the increase of the latter Lu−O_1 values (while this DI decreased) and the relatively smaller M−N_1 $\nabla^2\rho$ values for all complexes.

The overall stabilities of the gas-phase complexes, expressed by the Gibbs free energies of dissociation to $M^{3+} + L^{2-}$ (Table 1), are determined by an interplay of covalent (CT by spatial orbital overlap and energy-degeneracy-driven covalency,[68,82−86] the latter difficult to estimate quantitatively) and ionic interactions as well as the strain energy of L^{2-} in the complex. The lowest stability of the $Ac(L)^+$ molecule is in agreement with the rather weak CT interactions, which seemingly could not efficiently be compensated by the stronger ionic interactions and the weakest ligand strain in this complex. The promoting effect of short bond distances appears in the largest dissociation energy of $Lu(L)^+$ in spite of the weak CT and largest strain of the ligand but compensated effectively by the strong ionic interactions (cf. q_M in Table 1). The latter factor may mainly be responsible for the larger stability of the $Cf(L)^+$ molecule with respect to $La(L)^+$.

Regarding the two analyzed conformers, both the QTAIM and NBO results indicate a somewhat stronger CT in the $\Delta(\lambda\delta\lambda)(\lambda\delta\lambda)$ conformers compared to $\Delta(\delta\lambda\delta)(\delta\lambda\delta)$. The bond distances in Figure 3 are inconsistent in this respect, but most of them are shorter in the $\Delta(\lambda\delta\lambda)(\lambda\delta\lambda)$ conformers. Another characteristic feature is the negligible difference between the bonding parameters of the two $Ac(L)^+$ conformers in spite of their distinct energy difference. The very close bonding parameters are in accordance with the nearly identical Ac−O and Ac−N distances in the two conformers (vide supra).

Energetics in Aqueous Solution. One of the main issues regarding the medical application of metal complexes is the stability in aqueous solution. The stability of Ln(macropa) complexes is well explored. Stability constants have been obtained by potentiometric titration for the whole Ln series (except for the radioactive Pm).[34] They revealed a gradually decreasing stability from Ce ≈ La to Lu in contrast to complexes with popular ligands such as ethylenediaminetetraacetic acid ($EDTA^{4-}$) and derivatives[87,88] and the macrocyclic 1,4,7,10-tetraazacyclododecane-1,4,7,10-tetraacetic acid ($DOTA^{4-}$) and derivatives.[23,89]

The relative stabilities of the $M(L)^+$ complexes can be evaluated from the Gibbs free energies of the following exchange reaction (applicable for both gas phase and solution)

$$M_a(L)^+ + M_b^{3+} \rightarrow M_b(L)^+ + M_a^{3+} \quad (1)$$

The experimental stability trend for Ln(macropa) complexes in aqueous solution has been reproduced by Regueiro-Figueroa et al. using DFT calculations.[40] They revealed that the hydration energies of the Ln^{3+} ions have a crucial role in the delicate equilibrium of (1). While the calculated gas-phase Gibbs free energies indicated a preference of $Lu(L)^+$ by 372 kJ/mol with respect to $La(L)^+$, the calculated stability order was reversed in aqueous solution. The calculated hydration energies of the $Ln(L)^+$ complexes proved to be nearly the same for the whole Ln series.[40] On the other hand, the (experimental) hydration energy of the Lu^{3+} ion is higher by 419 kJ/mol than that of La^{3+}.[90,91] This larger stabilization of the Lu^{3+} ion in water shifted the equilibrium in (1) to the $La(L)^+ + Lu^{3+}$ side, facilitating in this way the thermodynamic preference of the $La(L)^+$ complex in aqueous solution. The obtained Gibbs free energy of −46.5 kJ/mol for the Lu → La exchange reaction was in good agreement with the experimental value of −38.5 kJ/mol.[40]

For the reproduction of the above experimental stability trend in aqueous solution, a crucial factor was the use of appropriate ionic radii in the hydration energy calculations of both the Ln^{3+} ions and their complexes. Calculations using the crystal[81] or experimental solution Ln^{3+} ionic radii (evaluated from the ion−water distances from extended X-ray absorption fine structure data[92]) in conjunction with the PCM/SMD model resulted in large deviations from the experimental hydration free energies. Regueiro-Figueroa et al. developed a parametrized set of Ln^{3+} radii for SMD calculations[40] by fitting to the experimental hydration free energy values.[90,91] This set was adapted to the TPSSh/LCPP theoretical level but comparable results were obtained with other DFT functionals, MP2, and the all-electron second-order Douglas−Kroll−Hess (DKH2) method too. Somewhat larger deviations were noted for the SCPP pseudopotentials.[40]

In the present study, the calculated Gibbs free energy of the Lu → La exchange reaction 1 was successfully reproduced

https://dx.doi.org/10.1021/acsomega.0c02873
ACS Omega 2020, 5, 26431−26440

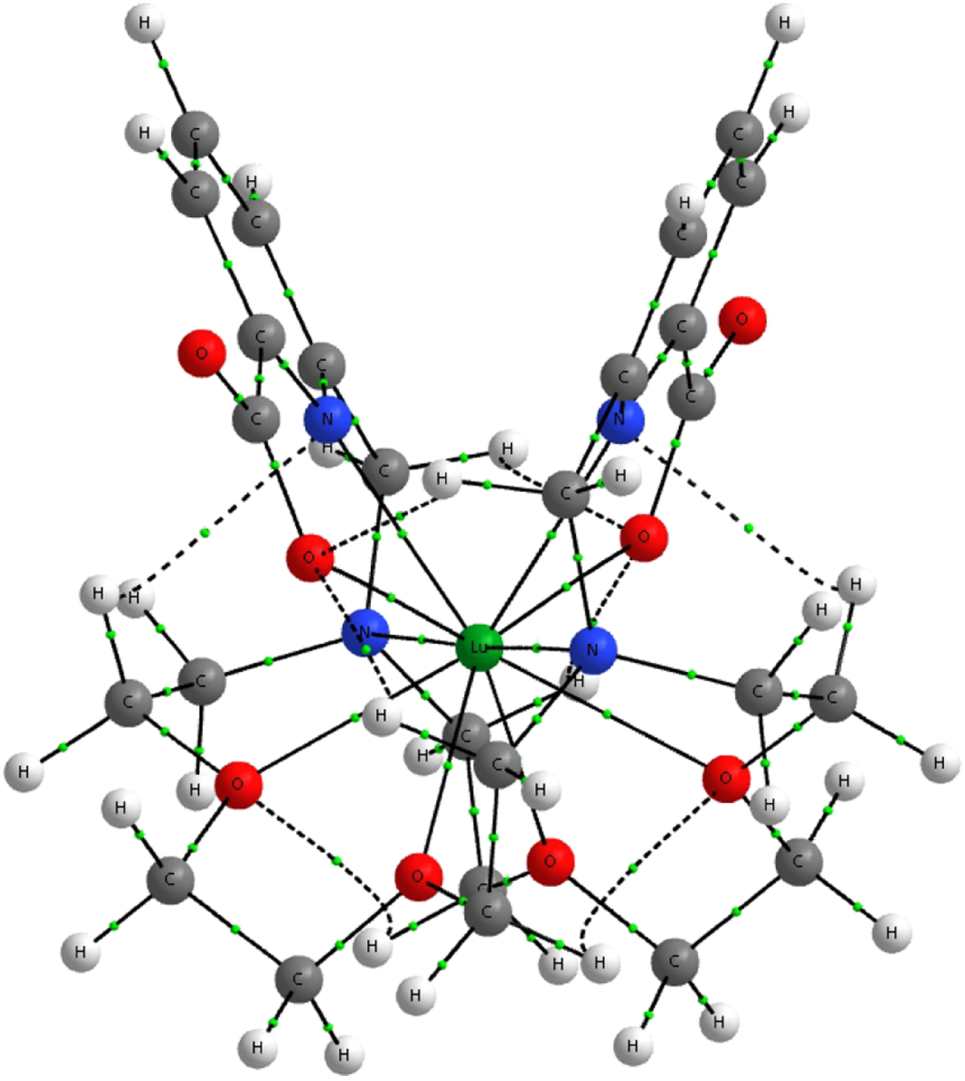

Figure 6. Bond critical points from QTAIM analysis of the $\Delta(\lambda\delta\lambda)(\lambda\delta\lambda)$ conformer of $Lu(L)^+$.

(−46.2 kJ/mol) by calculations on the $\Delta(\delta\lambda\delta)(\delta\lambda\delta)$ conformers at the (same) TPSSh/LCPP level using the PCM radii from ref 40. It should be noted, however, that the $\Delta(\delta\lambda\delta)(\delta\lambda\delta)$ conformer used in ref 40 (and similarly in ref 56) is not the most stable one in aqueous solution for $Lu(L)^+$. According to nuclear magnetic resonance (NMR) measurements, the smaller late Ln(macropa) complexes likely have a different conformation in solution than La(macropa). Moreover, the paramagnetic ^{1}H NMR shifts measured for Yb(macropa) indicated the preference of the $\Delta(\lambda\delta\lambda)(\lambda\delta\lambda)$ conformation in water.[34] The previously mentioned DFT studies included only the $\Delta(\delta\lambda\delta)$-$(\delta\lambda\delta)$ conformers and did not consider the $\Delta(\lambda\delta\lambda)(\lambda\delta\lambda)$ forms.[40,56] Calculations in this work at the TPSSh/LCPP + SMD level predicted a preference of the $\Delta(\delta\lambda\delta)(\delta\lambda\delta)$ conformer of $La(L)^+$ over the $\Delta(\lambda\delta\lambda)(\lambda\delta\lambda)$ conformer of $Lu(L)^+$ by 54.4 kJ/mol. Hence, for the more likely $\Delta(\lambda\delta\lambda)(\lambda\delta\lambda)$ conformer, the applied DFT level[40] produces a somewhat larger deviation from the experimental value of 38.5 kJ/mol. At the TPSSh/SCPP + SMD level, the preference of $La(L)^+$ is even larger, 63.3 kJ/mol.

Another noteworthy issue is the prediction of the energetic order of the two conformers of $Lu(L)^+$ in solution by the applied DFT + SMD model. As can be seen in Figure 2, in aqueous solution, the computed $\Delta(\delta\lambda\delta)(\delta\lambda\delta)$ conformer became superior to the $\Delta(\lambda\delta\lambda)(\lambda\delta\lambda)$ one, in contrast to available experimental information on Ln(macropa) complexes (vide supra).[34] Altogether, while recognizing the merits of this complex theoretical model (consisting of the TPSSh functional, SMD solvation model, and PCM radii for Ln^{3+}) on reproducing the experimental stability trend of $Ln(L)^+$ complexes in aqueous solution, the reliability of the predicted energy values is still restricted. In the view of the shown performance of the DFT calculations, (only) a qualitative assessment is reasonable for the thermodynamic properties of the present $An(L)^+$ complexes.

For the Ac^{3+} and Cf^{3+} ions, no experimental hydration energies are available. They were calculated on the basis of the ionic model by Bratsch and Lagowski[61,93−95] and by David.[96] The ΔG^0_{hyd} values from the two different model calculations differ considerably. From the two literature sources, the one by Bratsch and Lagowski[56,85] was chosen here because their ΔG^0_{hyd} results for Ln^{3+} ions[93,95] (after correction for the new standard Gibbs free hydration energy of proton[91]) achieved excellent agreement[40] with the experimental data.[90,97] The literature hydration energies of Ac^{3+} and Cf^{3+} were also corrected here for the new ΔG^0_{hyd} of H^+ according to (2)[40,45] and then used as a reference for the development of the PCM radii of these ions.

https://dx.doi.org/10.1021/acsomega.0c02873
ACS Omega 2020, 5, 26431−26440

$$\Delta G^0{}_{hyd}(M^{3+}) = \Delta G^0{}_{hyd}(M^{3+}) + 3(-1066.3) - 3(-1104.8)\ kJ/mol \quad (2)$$

The PCM radii of hydrated Ac^{3+} and Cf^{3+} were obtained here by SMD calculations, applying a correction on the calculated ΔG^0 values for the concentration change between the gas and liquid phase (7.83 kJ/mol under standard conditions).[40] The thus obtained PCM radii for Ac^{3+} and Cf^{3+} were 1.933 and 1.747 Å, respectively, with both the LCPPs and SCPPs. They are depicted together with the ones of La^{3+} and Lu^{3+} from ref 40 and available crystal ionic radii[81] in Figure S4, where an approximately linear relationship can be recognized. The above PCM radii were used in the SMD calculations of the $Ac(L)^+$ and $Cf(L)^+$ complexes.

The calculated relative stabilities (ΔG^0) of the studied $M(L)^+$ conformers in water are given in Figure 2. The relative stabilities of the $Ac(L)^+$ complexes show only small variations in the gaseous and aqueous phases; the preferred stability of the $\Delta(\delta\lambda\delta)(\delta\lambda\delta)$ conformer was computed to be ca. 13 kJ/mol with respect to $\Delta(\lambda\delta\lambda)(\lambda\delta\lambda)$. In contrast, for the La, Cf, and Lu complexes, a considerable stabilization of the $\Delta(\delta\lambda\delta)(\delta\lambda\delta)$ conformer with respect to $\Delta(\lambda\delta\lambda)(\lambda\delta\lambda)$ was predicted by the theoretical model upon solvation. Similarly, a larger stability of the $\Delta(\delta\lambda\delta)(\delta\lambda\delta)$ conformer in aqueous solution with respect to the $\Delta(\lambda\delta\lambda)(\lambda\delta\lambda)$ conformer has been recently obtained at the same theoretical level for $Ln(CHX\text{-}L)^+$ complexes, where CHX-L is a slightly modified rigid analogue of macropa.[56] In the view of the abovementioned NMR results on Ln(macropa) complexes,[34] the predicted stabilizations of the $\Delta(\delta\lambda\delta)(\delta\lambda\delta)$ conformers are likely overestimated. Accordingly, here, the predicted preference of the $\Delta(\delta\lambda\delta)(\delta\lambda\delta)$ conformer of $Cf(L)^+$ is ambiguous.

From the point of view of medical application, the main question is the stability of the $Ac(L)^+$ and $Cf(L)^+$ complexes in aqueous solution. In Table 2, the computed ΔG^0_{aq} data of the exchange reaction 1 are presented using the $\Delta(\delta\lambda\delta)(\delta\lambda\delta)$ conformer of $La(L)^+$ as reference. Because of the lack of BSSE corrections for $Ac(L)^+$ and $Cf(L)^+$ with SCPP, data with both pseudopotentials, furthermore with and without BSSE correction, are presented. According to the available data, correction for BSSE can stabilize the complexes with respect to $La(L)^+$ by 4−15 kJ/mol.

Table 2. Relative Stabilities of $M(L)^+$ Complexes in Aqueous Solution in Terms of ΔG^0_{aq} (kJ/mol) of the Exchange Reaction 1[a]

method	conformer[b]	$Ac(L)^+$	$La(L)^+$	$Cf(L)^+$	$Lu(L)^+$[c]
LCPP + BSSE	$\delta\lambda\delta$	8.4	0.0	43.6	46.2
	$\lambda\delta\lambda$	21.1	28.3	51.9	54.4
SCPP + BSSE	$\delta\lambda\delta$		0.0		58.0
	$\lambda\delta\lambda$		22.7		63.3
LCPP	$\delta\lambda\delta$	13.9	0.0	52.3	56.2
	$\lambda\delta\lambda$	25.4	30.7	65.1	69.9
SCPP	$\delta\lambda\delta$	26.2	0.0	34.8	69.7
	$\lambda\delta\lambda$	38.6	24.5	39.6	77.4

[a]Reference is the $\Delta(\delta\lambda\delta)(\delta\lambda\delta)$ conformer of $La(L)^+$. [b]The conformers $\Delta(\delta\lambda\delta)(\delta\lambda\delta)$ and $\Delta(\lambda\delta\lambda)(\lambda\delta\lambda)$ are denoted by $\delta\lambda\delta$ and $\lambda\delta\lambda$, respectively. [c]The experimental value is 38.5 kJ/mol.[40]

The data predict $Ac(L)^+$ and $Cf(L)^+$ relative stabilities between $La(L)^+$ and $Lu(L)^+$ in aqueous solution (cf. Table 2). In agreement with the expectation, the stability of $Ac(L)^+$ is close to that of $La(L)^+$. The computed high thermodynamic stability of $Ac(L)^+$ extends the experimental observations on the outstanding kinetic stability of Ac(macropa), according to which the complex did not release Ac^{3+} in vivo and 98% of it remained intact against excess La^{3+} over 7−8 days.[33]

The LCPP and SCPP results show larger differences for $Cf(L)^+$: the former theoretical level predicted stability close to $Lu(L)^+$ while the latter a considerably higher one in between $La(L)^+$ and $Lu(L)^+$. The source of this difference is the considerably smaller hydration energy of the $Cf(L)^+$ complex calculated with SCPP.

CONCLUSIONS

In the present study, the complex formation of four f elements (La and Lu with 4f valence subshell and Ac and Cf with 5f valence subshell) with the 18-membered macrocycle macropa ligand was compared. While all four metals have isotopes with potential radiotherapeutic applications, the greatest interest presently is in finding a suitable chelator ligand for Ac. The bonding interactions in the complexes were analyzed on the basis of characteristic geometrical parameters, topological properties of the electron density distribution, natural atomic charges, and properties of CT interactions based on the NBO model.

For the gaseous phase, the DFT computations predicted very weak charge-transfer interactions in $Ac(L)^+$, which could not efficiently be compensated by the stronger ionic interactions and the weakest strain of L in this complex, resulting in the lowest stability of $Ac(L)^+$ from the four complexes. The largest dissociation energy was obtained for $Lu(L)^+$, in which the strong (short distance) ionic interactions could compensate effectively for the weak CT and largest strain of the L ligand. The strong ionic interactions (due again to the relatively short bond distances) could be suggested to be responsible for the larger stability of the $Cf(L)^+$ molecule with respect to $La(L)^+$, in spite of the strongest computed CT interactions in the latter complex.

The present results demonstrated the strong effect of water solvent on the thermodynamic equilibria of metal complexes. As a major effect, the large differences in the hydration energies of the M^{3+} ions play a crucial role in the ion exchange reactions of these $M(L)^+$ complexes. Altogether, the computations predicted comparable stability of $Ac(L)^+$ and $Cf(L)^+$ complexes to those of the $Ln(L)^+$ ones in aqueous solution, in agreement with experimental observations on $Ac(L)^+$. The stability of $Ac(L)^+$ was predicted to be somewhat lower than that of $La(L)^+$, while the stability of the smaller $Cf(L)^+$ was even lower but still higher than that of $Lu(L)^+$. These stabilities support a potential medical application of these actinides.

ASSOCIATED CONTENT

Supporting Information

The Supporting Information is available free of charge at https://pubs.acs.org/doi/10.1021/acsomega.0c02873.

Relative Gibbs free energies of the eight $M(L)^+$ complexes in the gaseous phase and aqueous solution; selected bond distances and topological properties of the $\Delta(\delta\lambda\delta)(\delta\lambda\delta)$ and $\Delta(\lambda\delta\lambda)(\lambda\delta\lambda)$ conformers; figures on the strain energy of the ligand, electron density distribution, and Laplacian of the electron density distribution at selected bond critical points; PCM radii; Cartesian coordinates of the

https://dx.doi.org/10.1021/acsomega.0c02873
ACS Omega 2020, 5, 26431−26440

$Ac(L)^+$ and $Cf(L)^+$ conformers optimized at the TPSSh/SCPP level (PDF)

AUTHOR INFORMATION

Corresponding Author

Attila Kovács − *Joint Research Centre, European Commission, D-76125 Karlsruhe, Germany;* orcid.org/0000-0001-8169-3547; Phone: +49-7247-951842; Email: attila.kovacs@ec.europa.eu

Complete contact information is available at: https://pubs.acs.org/10.1021/acsomega.0c02873

Notes

The author declares no competing financial interest.

ACKNOWLEDGMENTS

The author thanks Dr. A. Morgenstern for advice.

REFERENCES

(1) Geerlings, M. W.; Kaspersen, F. M.; Apostolidis, C.; Van Der Hout, R. The feasibility of ^{225}Ac as a source of α-particles in radioimmunotherapy. *Nucl. Med. Commun.* **1993**, *14*, 121−125.

(2) Miederer, M.; Scheinberg, D. A.; McDevitt, M. R. Realizing the potential of the Actinium-225 radionuclide generator in targeted alpha particle therapy applications. *Adv. Drug Delivery Rev.* **2008**, *60*, 1371−1382.

(3) Thiele, N. A.; Wilson, J. J. Actinium-225 for targeted α therapy: Coordination chemistry and current chelation approaches. *Cancer Biother. Radiopharm.* **2018**, *33*, 336−348.

(4) Morgenstern, A.; Apostolidis, C.; Kratochwil, C.; Sathekge, M.; Krolicki, L.; Bruchertseifer, F. An overview of targeted alpha therapy with ^{225}Actinium and ^{213}Bismuth. *Curr. Radiopharm.* **2018**, *11*, 200−208.

(5) Henriksen, G.; Bruland, Ø. S.; Larsen, R. H. Thorium and Actinium Polyphosphonate Compounds As Bone-seeking Alpha Particle-emitting Agents. *Anticancer Res.* **2004**, *24*, 101−105.

(6) Dahle, J.; Borrebæk, J.; Jonasdottir, T. J.; Hjelmerud, A. K.; Melhus, K. B.; Bruland, Ø. S.; Press, O. W.; Larsen, R. H. Targeted cancer therapy with a novel low-dose rate α-emitting radioimmunoconjugate. *Blood* **2007**, *110*, 2049−2056.

(7) Dahle, J.; Larsen, R. H. Targeted alpha-particle therapy with ^{227}Th-labeled antibodies. *Curr. Radiopharm.* **2008**, *1*, 209−214.

(8) Abbas, N.; Heyerdahl, H.; Bruland, Ø. S.; Borrebæk, J.; Nesland, J.; Dahle, J. Experimental α-particle radioimmunotherapy of breast cancer using ^{227}Th-labeled p-benzyl-DOTA-trastuzumab. *EJNMMI Res.* **2011**, *1*, No. 18.

(9) Kratochwil, C.; Bruchertseifer, F.; Giesel, F. L.; Weis, M.; Verburg, F. A.; Mottaghy, F.; Kopka, K.; Apostolidis, C.; Haberkorn, U.; Morgenstern, A. ^{225}Ac-PSMA-617 for PSMA-targeted a-radiation therapy of metastatic castration-resistant prostate cancer. *J. Nucl. Med.* **2016**, *57*, 1941−1944.

(10) Kratochwil, C.; Bruchertseifer, F.; Rathke, H.; Bronzel, M.; Apostolidis, C.; Weichert, W.; Haberkorn, U.; Giesel, F. L.; Morgenstern, A. Targeted α-therapy of metastatic castration-resistant prostate cancer with ^{225}Ac-PSMA-617: Dosimetry estimate and empiric dose finding. *J. Nucl. Med.* **2017**, *58*, 1624−1631.

(11) Hammer, S.; Hagemann, U. B.; Zitzmann-Kolbe, S.; Larsen, A.; Ellingsen, C.; Geraudie, S.; Grant, D.; Indrevoll, B.; Smeets, R.; von Ahsen, O.; et al. Preclinical Efficacy of a PSMA-Targeted Thorium-227 Conjugate (PSMA-TTC), a Targeted Alpha Therapy for Prostate Cancer. *Clin. Cancer Res.* **2020**, *26*, 1985−1996.

(12) Jurcic, J. G.; Rosenblat, T. L.; McDevitt, M. R.; Pandit-Taskar, N.; Carrasquillo, J. A.; Chanel, S. M.; Zikaras, K.; Frattini, M. G.; Maslak, P. M.; Cicic, D.; et al. Targeted Alpha-Particle Nano-Generator Actinium-225 (^{225}Ac)-Lintuzumab (Anti-CD33) in Acute Myeloid Leukemia (AML). *Clin. Lymphoma, Myeloma Leuk.* **2013**, *13*, S379−S380.

(13) Jurcic, J. G.; Ravandi, F.; Pagel, J. M.; Park, J. H.; Smith, B. D.; Douer, D.; Levy, M. Y.; Estey, E.; Kantarjian, H. M.; Earle, D.; et al. Phase I trial of α-particle therapy with actinium-225 (^{225}Ac)-lintuzumab (anti-CD33) and low-dose cytarabine (LDAC) in older patients with untreated acute myeloid leukemia (AML.). *J. Clin. Oncol.* **2015**, *33*, 7050.

(14) Kratochwil, C.; Bruchertseifer, F.; Giesel, F.; Apostolidis, C.; Haberkorn, U.; Morgenstern, A. Ac-225-DOTATOC - an Empiric Dose Finding for Alpha Particle Emitter Based Radionuclide Therapy of Neuroendocrine Tumors. *J. Nucl. Med.* **2015**, *56*, 1232.

(15) Hagemann, U. B.; Ellingsen, C.; Schuhmacher, J.; Kristian, A.; Mobergslien, A.; Cruciani, V.; Wickstroem, K.; Schatz, C. A.; Kneip, C.; Golfier, S.; et al. Mesothelin-Targeted Thorium-227 Conjugate (MSLN-TTC): Preclinical Evaluation of a New Targeted Alpha Therapy for Mesothelin-Positive Cancers. *Clin. Cancer Res.* **2019**, *25*, 4723−4734.

(16) Morgenstern, A.; Apostolidis, C.; Bruchertseifer, F.; Capote, R.; Gouder, T.; Simonelli, F.; Sin, M.; Abbas, K. Cross-sections of the reaction 232Th(p,3n)230Pa for production of 230U for targeted alpha therapy. *Appl. Radiat. Isot.* **2008**, *66*, 1275−1280.

(17) Montavon, G.; Apostolidis, C.; Bruchertseifer, F.; Repinc, U.; Morgenstern, A. Spectroscopic study of the interaction of U(VI) with transferrin and albumin for speciation of U(VI) under blood serum conditions. *J. Inorg. Biochem.* **2009**, *103*, 1609−1616.

(18) Montavon, G.; Repinc, U.; Apostolidis, C.; Bruchertseifer, F.; Abbas, K.; Morgenstern, A. Investigation of para-sulfonatocalix[n]-arenes [n = 6, 8] as potential chelates for ^{230}U. *Dalton Trans.* **2010**, *39*, 1366−1374.

(19) Schlea, C. S.; Stoddard, D. H. Californium Isotopes Proposed for Intracavity and Interstitial Radiation Therapy with Neutrons. *Nature* **1965**, *206*, 1058−1059.

(20) Wang, C.-K. C. Progress in Californium-252 Neutron Brachytherapy. In *Brachytherapy*; Kishi, K., Ed.; InTech: Rijeka, Croatia, 2012; pp 33−58.

(21) Price, E. W.; Orvig, C. Matching chelators to radiometals for radiopharmaceuticals. *Chem. Soc. Rev.* **2014**, *43*, 260−290.

(22) Cacheris, W. P.; Nickle, S. K.; Sherry, A. D. Thermodynamic study of lanthanide complexes of 1,4,7-triazacyclononane-N,N′,N″-triacetic acid and 1,4,7,10-tetraazacyclododecane-N,N′,N″,N‴-tetra-acetic acid. *Inorg. Chem.* **1987**, *26*, 958−960.

(23) Clarke, E. T.; Martell, A. E. Stabilities of trivalent metal ion complexes of the tetraacetate derivatives of 12-, 13- and 14-membered tetraazamacrocycles. *Inorg. Chim. Acta* **1991**, *190*, 37−46.

(24) Morgenstern, A.; Apostolidis, C.; Bruchertseifer, F. Supply and Clinical Application of Actinium-225 and Bismuth-213. *Semin. Nucl. Med.* **2020**, *50*, 119−123.

(25) Chang, C. A.; Rowland, M. E. Metal complex formation with 1,10-diaza-4,7,13,16-tetraoxacyclooctadecane-N,N′-diacetic acid. An approach to potential lanthanide ion selective reagents. *Inorg. Chem.* **1983**, *22*, 3866−3869.

(26) Damu, K. V.; Shaikjee, M. S.; Michael, J. P.; Howard, A. S.; Hancock, R. D. Control of metal ion selectivity in ligands containing neutral oxygen and pyridyl groups. *Inorg. Chem.* **1986**, *25*, 3879−3883.

(27) Hancock, R. D.; Bhavan, R.; Wade, P. W.; Boeyens, J. C. A.; Dobson, S. M. Ligand design for complexation in aqueous solution. 1. Neutral oxygen donor bearing groups as a means of controlling size-based selectivity for metal ions. *Inorg. Chem.* **1989**, *28*, 187−194.

(28) Brücher, E.; Györi, B.; Emri, J.; Solymosi, P.; Sztanyik, L. B.; Varga, L. 1,10-Diaza-4,7,13,16-tetraoxacyclooctadecane-1,10-bis-(malonate), a ligand with high Sr^{2+}/Ca^{2+} and Pb^{2+}/Zn^{2+} selectivities in aqueous solution. *J. Chem. Soc., Chem. Commun.* **1993**, 574−575.

(29) Zhang, X. X.; Bordunov, A. V.; Bradshaw, J. S.; Dalley, N. K.; Kou, X.; Izatt, R. M. A New Highly Selective Macrocycle for K^+ and Ba^{2+}: Effect of Formation of a Pseudo Second Macroring through Complexation. *J. Am. Chem. Soc.* **1995**, *117*, 11507−11511.

(30) Su, N.; Bradshaw, J. S.; Zhang, X. X.; Song, H.; Savage, P. B.; Xue, G.; Krakowiak, K. E.; Izatt, R. M. Syntheses and Metal Ion

Complexation of Novel 8-Hydroxyquinoline-Containing Diaza-18-Crown-6 Ligands and Analogues. *J. Org. Chem.* **1999**, *64*, 8855−8861.
(31) Jensen, M. P.; Chiarizia, R.; Shkrob, I. A.; Ulicki, J. S.; Spindler, B. D.; Murphy, D. J.; Hossain, M.; Roca-Sabio, A.; Platas-Iglesias, C.; de Blas, A.; et al. Aqueous Complexes for Efficient Size-based Separation of Americium from Curium. *Inorg. Chem.* **2014**, *53*, 6003−6012.
(32) Regueiro-Figueroa, M.; Barriada, J. L.; Pallier, A.; Esteban-Gómez, D.; de Blas, A.; Rodríguez-Blas, T.; Tóth, É.; Platas-Iglesias, C. Stabilizing Divalent Europium in Aqueous Solution Using Size-Discrimination and Electrostatic Effects. *Inorg. Chem.* **2015**, *54*, 4940−4952.
(33) Thiele, N. A.; Brown, V.; Kelly, J. M.; Amor-Coarasa, A.; Jermilova, U.; MacMillan, S. N.; Nikolopoulou, A.; Ponnala, S.; Ramogida, C. F.; Robertson, A. K. H.; et al. An Eighteen-Membered Macrocyclic Ligand for Actinium-225 Targeted Alpha Therapy. *Angew. Chem., Int. Ed.* **2017**, *56*, 14712−14717.
(34) Roca-Sabio, A.; Mato-Iglesias, M.; Esteban-Gómez, D.; Tóth, É.; de Blas, A.; Platas-Iglesias, C.; Rodríguez-Blas, T. Macrocyclic Receptor Exhibiting Unprecedented Selectivity for Light Lanthanides. *J. Am. Chem. Soc.* **2009**, *131*, 3331−3341.
(35) Ferreirós-Martínez, R.; Esteban-Gómez, D.; Tóth, E.; de Blas, A.; Platas-Iglesias, C.; Rodríguez-Blas, T. Macrocyclic receptor showing extremely high Sr(II)/Ca(II) and Pb(II)/Ca(II) selectivities with potential application in chelation treatment of metal intoxication. *Inorg. Chem.* **2011**, *50*, 3772−3784.
(36) Thiele, N. A.; MacMillan, S. N.; Wilson, J. J. Rapid Dissolution of $BaSO_4$ by Macropa, an 18-Membered Macrocycle with High Affinity for Ba^{2+}. *J. Am. Chem. Soc.* **2018**, *140*, 17071−17078.
(37) Roca-Sabio, A.; Mato-Iglesias, M.; Esteban-Gómez, D.; de Blas, A.; Rodríguez-Blas, T.; Platas-Iglesias, C. The effect of ring size variation on the structure and stability of lanthanide(III) complexes with crown ethers containing picolinate pendants. *Dalton Trans.* **2011**, *40*, 384−392.
(38) Chang, C. A.; Ochaya, V. O. Potential Lanthanide Ion Selective Reagents. 3.1,2 Metal Complex Formation with l,7-Diaza-4,10,13-trioxacyclopentadecane-N,N/-diacetic Acid. *Inorg. Chem.* **1986**, *25*, 355−358.
(39) Kelly, J. M.; Amor-Coarasa, A.; Ponnala, S.; Nikolopoulou, A.; Williams, C.; Thiele, N. A.; Schyler, D.; Wilson, J. J.; DiMagno, S. G.; Babich, J. W. A Single Dose of ^{225}Ac-RPS-074 Induces a Complete Tumor Response in a LNCaP Xenograft Model. *J. Nucl. Med.* **2019**, *60*, 649−655.
(40) Regueiro-Figueroa, M.; Esteban-Gómez, D.; de Blas, A.; Rodríguez-Blas, T.; Platas-Iglesias, C. Understanding Stability Trends along the Lanthanide Series. *Chem. − Eur. J.* **2014**, *20*, 3974−3981.
(41) Bhavan, R.; Hancock, R. D.; Wade, P. W.; Boeyens, J. C. A.; Dobson, S. M. Crystallographic study of the barium(II) complex of a lariat ether with long pendent arms. *Inorg. Chim. Acta* **1990**, *171*, 235−238.
(42) Hancock, R. D.; Siddons, C. J.; Oscarson, K. A.; Reibenspies, J. M. The structure of the 11-coordinate barium complex of the pendant-donor macrocycle 1,4,7,10-tetrakis(carbamoylmethyl)−1,4,7,10-tetraazacyclododecane: an analysis of the coordination numbers of barium(II) in its complexes. *Inorg. Chim. Acta* **2004**, *357*, 723−727.
(43) Frisch, M. J.; Trucks, G. W.; Schlegel, H. B.; Scuseria, G. E.; Robb, M. A.; Cheeseman, J. R.; Scalmani, G.; Barone, V.; Mennucci, B.; Petersson, G. A. et al. *Gaussian 09*, revision D.01; Gaussian, Inc.: Wallingford, CT, 2010.
(44) Tao, J.; Perdew, J. P.; Staroverov, V. N.; Scuseria, G. E. Climbing the density functional ladder: Nonempirical meta-generalized gradient approximation designed for molecules and solids (TPSSTPSS). *Phys. Rev. Lett.* **2003**, *91*, No. 146401.
(45) Roca-Sabio, A.; Regueiro-Figueroa, M.; Esteban-Gómez, D.; de Blas, A.; Rodríguez-Blas, T.; Platas-Iglesias, C. Density functional dependence of molecular geometries in lanthanide(III) complexes relevant to bioanalytical and biomedical applications. *Comput. Theor. Chem.* **2012**, *999*, 93−104.
(46) Huang, P.-W. Understanding the Stability Trend Along Light Lanthanide Complexes with an Ehtylenediamine-Type Ligand: A Quantum Chemical Study. *ChemistrySelect* **2019**, *4*, 12368−12374.
(47) Esteban-Gómez, D.; de Blas, A.; Rodríguez-Blas, T.; Helm, L.; Platas-Iglesias, C. Hyperfine coupling constants on inner-sphere water molecules of Gd III-based MRI contrast agents. *ChemPhysChem* **2012**, *13*, 3640−3650.
(48) Dolg, M.; Stoll, H.; Savin, A.; Preuss, H. Energy-adjusted pseudopotentials for the rare earth elements. *Theor. Chim. Acta* **1989**, *75*, 173−194.
(49) Dolg, M.; Stoll, H.; Preuss, H. A combination of quasirelativistic pseudopotential and ligand field calculations for lanthanoid compounds. *Theor. Chim. Acta* **1993**, *85*, 441−450.
(50) Cao, X.; Dolg, M. Valence basis sets for relativistic energy-consistent small-core lanthanide pseudopotentials. *J. Chem. Phys.* **2001**, *115*, 7348−7355.
(51) Cao, X.; Dolg, M. Segmented contraction scheme for small-core lanthanide pseudopotential basis sets. *J. Mol. Struct.: THEOCHEM* **2002**, *581*, 139−147.
(52) Küchle, W.; Dolg, M.; Stoll, H.; Preuss, H. Energy-Adjusted Pseudopotentials for the Actinides. Parameter Sets and Test Calculations for Thorium and Thorium Monoxide. *J. Chem. Phys.* **1994**, *100*, 7535−7542.
(53) Cao, X.; Dolg, M.; Stoll, H. Valence basis sets for relativistic energy-consistent small-core actinide pseudopotentials. *J. Chem. Phys.* **2003**, *118*, 487−496.
(54) Cao, X.; Dolg, M. Segmented contraction scheme for small-core actinide pseudopotential basis sets. *J. Mol. Struct.: THEOCHEM* **2004**, *673*, 203−209.
(55) Moritz, A.; Cao, X.; Dolg, M. Quasirelativistic energy-consistent 5f-in-core pseudopotentials for trivalent actinide elements. *Theor. Chem. Acc.* **2007**, *117*, 473−481.
(56) Thiele, N. A.; Woods, J. J.; Wilson, J. J. Implementing f-Block Metal Ions in Medicine: Tuning the Size Selectivity of Expanded Macrocycles. *Inorg. Chem.* **2019**, *58*, 10483−10500.
(57) Boys, S. F.; Bernardi, F. The calculation of small molecular interactions by the differences of separate total energies. Some procedures with reduced errors. *Mol. Phys.* **1970**, *19*, 553−566.
(58) Tomasi, J.; Mennucci, B.; Cammi, R. Quantum mechanical continuum solvation models. *Chem. Rev.* **2005**, *105*, 2999−3093.
(59) Scalmani, G.; Frisch, M. J. Continuous surface charge polarizable continuum models of solvation. I. General formalism. *J. Chem. Phys.* **2010**, *132*, No. 114110.
(60) Marenich, A. V.; Cramer, C. J.; Truhlar, D. G. Universal Solvation Model Based on Solute Electron Density and on a Continuum Model of the Solvent Defined by the Bulk Dielectric Constant and Atomic Surface Tensions. *J. Phys. Chem. B* **2009**, *113*, 6378−6396.
(61) Choppin, G. R.; Jensen, M. P. Actinides in Solution: Complexation and Kinetics. In *The Chemistry of the Actinide and Transactinide Elements*; Morss, L. R.; Edelstein, N. M.; Fuger, J., Eds.; Springer: Dordrecht, 2006; Vol. 4, pp 2539−2540.
(62) Reed, A. E.; Curtiss, L. A.; Weinhold, F. Intermolecular interactions from a natural bond orbital, donor-acceptor viewpoint. *Chem. Rev.* **1988**, *88*, 899−926.
(63) Glendening, E. D.; Landis, C. R.; Weinhold, F. NBO 6.0: Natural Bond Orbital Analysis Program. *J. Comput. Chem.* **2013**, *34*, 1429−1437.
(64) Bader, R. F. W. *Atoms in Molecules. A Quantum Theory*; Oxford University Press: Oxford, 1990.
(65) Keith, T. A. *AIMAll (Version 17.11.14)*; TK Gristmill Software: Overland Park, 2017.
(66) Hayton, T. W.; Kaltsoyannis, N. Organometallic Actinide Complexes with Novel Oxidation States and Ligand Types. In *Experimental and Theoretical Approaches to Actinide Chemistry*; Gibson, J. K.; de Jong, W. A., Eds.; John Wiley & Sons, Inc.: Hoboken, New Jersey, 2018; pp 181−236.
(67) Kaltsoyannis, N. Transuranic Computational Chemistry. *Chem. − Eur. J.* **2018**, *24*, 2815−2825.

https://dx.doi.org/10.1021/acsomega.0c02873
ACS Omega 2020, 5, 26431−26440

(68) Kerridge, A. Quantification of f-element covalency through analysis of the electron density: insights from simulation. *Chem. Commun.* **2017**, *53*, 6685−6695.
(69) Dognon, J.-P. Theoretical insights into the chemical bonding in actinide complexes. *Coord. Chem. Rev.* **2014**, *266*−*267*, 110−122.
(70) Jones, M. B.; Gaunt, A. J.; Gordon, J. C.; Kaltsoyannis, N.; Neu, M. P.; Scott, B. L. Uncovering f-element bonding differences and electronic structure in a series of 1:3 and 1:4 complexes with a diselenophosphinate ligand. *Chem. Sci.* **2013**, *4*, 1189−1203.
(71) Schnaars, D. D.; Gaunt, A. J.; Hayton, T. W.; Jones, M. B.; Kirker, I.; Kaltsoyannis, N.; May, I.; Reilly, S. D.; Scott, B. L.; Wu, G. Bonding trends traversing the tetravalent actinide series: Synthesis, structural, and computational analysis of $An^{IV}(^{Ar}acnac)_4$ complexes (An = Th, U, Np, Pu; ^{Ar}acnac = ArNC(Ph)CHC(Ph)O; Ar = 3,5-$^{t}Bu_2C_6H_3$). *Inorg. Chem.* **2012**, *51*, 8557−8566.
(72) Kerridge, A. Oxidation state and covalency in f-element metallocenes (M = Ce, Th, Pu): A combined CASSCF and topological study. *Dalton Trans.* **2013**, *42*, 16428−16436.
(73) Kerridge, A. f-Orbital covalency in the actinocenes (An = Th−Cm): multiconfigurational studies and topological analysis. *RSC Adv.* **2014**, *4*, 12078−12086.
(74) Huang, Q. R.; Kingham, J. R.; Kaltsoyannis, N. The strength of actinide-element bonds from the quantum theory of atoms-in-molecules. *Dalton Trans.* **2015**, *44*, 2554−2566.
(75) Banik, N. L.; Vallet, V.; Réal, F.; Belmecheri, R. M.; Schimmelpfennig, B.; Rothe, J.; Marsac, R.; Lindqvist-Reis, P.; Walther, C.; Denecke, M. A.; et al. First structural characterization of Pa(iv) in aqueous solution and quantum chemical investigations of the tetravalent actinides up to Bk(iv): the evidence of a curium break. *Dalton Trans.* **2016**, *45*, 453−457.
(76) Kaltsoyannis, N. Covalency hinders $AnO_2(H_2O)^+ \rightarrow AnO(OH)_2^+$ isomerisation (An = Pa−Pu). *Dalton Trans.* **2016**, *45*, 3158−3162.
(77) Wu, Q. Y.; Cheng, Z. P.; Lan, J. H.; Wang, C. Z.; Chai, Z. F.; Gibson, J. K.; Shi, W. Q. Insight into the nature of M-C bonding in the lanthanide/actinide-biscarbene complexes: A theoretical perspective. *Dalton Trans.* **2018**, *47*, 12718−12725.
(78) Kovács, A.; Apostolidis, C.; Walter, O. Comparative study of complexes of rare earths and actinides with 2,6-bis(1,2,4-triazin-3-yl)pyridine. *Inorganics* **2019**, *7*, No. 26.
(79) Corey, E. J.; Bailar, J. C. The Stereochemistry of Complex Inorganic Compounds. XXII. Stereospecific Effects in Complex Ions. *J. Am. Chem. Soc.* **1959**, *81*, 2620−2629.
(80) Beattie, J. K. Conformational Analysis of Tris(ethylenediamine) Complexes. *Acc. Chem. Res.* **1971**, *4*, 253−259.
(81) Shannon, R. D. Revised Effective Ionic Radii and Systematic Studies of Interatomic Distances in Halides and Chalcogenides. *Acta Crystallogr.* **1976**, *A32*, 751−767.
(82) Kelley, M. P.; Su, J.; Urban, M.; Luckey, M.; Batista, E. R.; Yang, P.; Shafer, J. C. On the Origin of Covalent Bonding in Heavy Actinides. *J. Am. Chem. Soc.* **2017**, *139*, 9901−9908.
(83) Su, J.; Batista, E. R.; Boland, K. S.; Bone, S. E.; Bradley, J. A.; Cary, S. K.; Clark, D. L.; Conradson, S. D.; Ditter, A. S.; Kaltsoyannis, N.; et al. Energy-Degeneracy-Driven Covalency in Actinide Bonding. *J. Am. Chem. Soc.* **2018**, *140*, 17977−17984.
(84) Albrecht-Schmitt, T. E.; Hobart, D. E.; Páez-Hernández, D.; Celis-Barros, C. Theoretical examination of covalency in berkelium-(IV) carbonate complexes. *Int. J. Quantum Chem.* **2020**, *120*, No. e26254.
(85) Chandrasekar, A.; Ghanty, T. K. Uncovering Heavy Actinide Covalency: Implications for Minor Actinide Partitioning. *Inorg. Chem.* **2019**, *58*, 3744−3753.
(86) Kelley, M. P.; Deblonde, G. J. P.; Su, J.; Booth, C. H.; Abergel, R. J.; Batista, E. R.; Yang, P. Bond Covalency and Oxidation State of Actinide Ions Complexed with Therapeutic Chelating Agent 3,4,3-LI(1,2-HOPO). *Inorg. Chem.* **2018**, *57*, 5352−5363.
(87) Lacoste, R. G.; Christoffers, G. V.; Martell, A. E. New Multidentate Ligands. II. Amino Acids Containing α-Pyridyl Groups. *J. Am. Chem. Soc.* **1965**, *87*, 2385−2388.
(88) Tei, L.; Baranyai, Z.; Brücher, E.; Cassino, C.; Demicheli, F.; Masciocchi, N.; Giovenzana, G. B.; Botta, M. Dramatic increase of selectivity for heavy lanthanide(III) cations by tuning the flexibility of polydentate chelators. *Inorg. Chem.* **2010**, *49*, 616−625.
(89) Loncin, M. F.; Desreux, J. F.; Merciny, E. Coordination of Lanthanides by Two Polyamino Polycarboxylic Macrocycles: Formation of Highly Stable Lanthanide Complexes. *Inorg. Chem.* **1986**, *25*, 2646−2648.
(90) Guillaumont, R.; David, F. Fonctions thermodynamiques d'hydration et d'oxydo-reduction des ions M3+ des lanthanides. *Radiochem. Radioanal. Lett.* **1974**, *17*, 25−39.
(91) Cosentino, U.; Villa, A.; Pitea, D.; Moro, G.; Barone, V. Extension of computational chemistry to the study of lanthanide(III) ions in aqueous solution: Implementation and validation of a continuum solvent approach. *J. Phys. Chem. B* **2000**, *104*, 8001−8007.
(92) D'Angelo, P.; Zitolo, A.; Migliorati, V.; Chillemi, G.; Duvail, M.; Vitorge, P.; Abadie, S.; Spezia, R. Revised ionic radii of lanthanoid(III) ions in aqueous solution. *Inorg. Chem.* **2011**, *50*, 4572−4579.
(93) Bratsch, S. G.; Lagowski, J. J. Lanthanide thermodynamic predictions. 7. Thermodynamics of 2+, 3+, and 4+ aquo ions and standard electrode potentials at 298.15 K. *J. Phys. Chem. A.* **1985**, *89*, 3317−3319.
(94) Bratsch, S. G.; Lagowski, J. J. Actinide Thermodynamic Predictions. 3. Thermodynamlcs of Compounds and Aquo Ions of the 2+, 3+, and 4+ Oxidation States and Standard Electrode Potentials at 298.15 K. *J. Phys. Chem. B.* **1986**, *90*, 307−312.
(95) Bratsch, S. G.; Lagowski, J. J. Lanthanide thermodynamic predictions. 6. Thermodynamics of gas-phase ions and revised enthalpy equations for solids at 298.15 K. *J. Phys. Chem. C.* **1985**, *89*, 3310−3316.
(96) David, F. H. About low oxidation states, hydration and covalence properties of f elements. *Radiochim. Acta* **2008**, *96*, 135−144.
(97) Morss, L. R. Thermochemical properties of yttrium, lanthanum, and the lanthanide elements and ions. *Chem. Rev.* **1976**, *76*, 827−841.

https://dx.doi.org/10.1021/acsomega.0c02873
ACS Omega 2020, 5, 26431−26440